Potential energy surface, dipole moment surface and the intensity calculations for the 10 μm, 5 μm and 3 μm bands of ozone

Oleg L. Polyansky [a,b,*], Nikolai F. Zobov [b], Irina I. Mizus [b], Aleksandra A. Kyuberis [b], Lorenzo Lodi [a], Jonathan Tennyson [a,*]

[a] Department of Physics and Astronomy, University College London, Gower Street, London WC1E 6BT, United Kingdom
[b] Institute of Applied Physics, Russian Academy of Science, Ulyanov Street 46, Nizhny Novgorod 603950, Russia

ABSTRACT

Monitoring ozone concentrations in the Earth's atmosphere using spectroscopic methods is a major activity which undertaken both from the ground and from space. However there are long-running issues of consistency between measurements made at infrared (IR) and ultraviolet (UV) wavelengths. In addition, key O_3 IR bands at 10 μm, 5 μm and 3 μm also yield results which differ by a few percent when used for retrievals. These problems stem from the underlying laboratory measurements of the line intensities. Here we use quantum chemical techniques, first principles electronic structure and variational nuclear-motion calculations, to address this problem. A new high-accuracy *ab initio* dipole moment surface (DMS) is computed. Several spectroscopically-determined potential energy surfaces (PESs) are constructed by fitting to empirical energy levels in the region below 7000 cm^{-1} starting from an *ab initio* PES. Nuclear motion calculations using these new surfaces allow the unambiguous determination of the intensities of 10 μm band transitions, and the computation of the intensities of 10 μm and 5 μm bands within their experimental error. A decrease in intensities within the 3 μm is predicted which appears consistent with atmospheric retrievals. The PES and DMS form a suitable starting point both for the computation of comprehensive ozone line lists and for future calculations of electronic transition intensities.

1. Introduction

The ozone molecule, O_3, is an important constituent of the Earth's atmosphere. At high altitudes its ultraviolet (UV) absorption bands protect life from deadly solar UV radiation, while at low altitude ozone represents a dangerous, poisonous pollutant. Monitoring of ozone concentration in the Earth's atmosphere is thus a major and important activity [1] which undertaken both from the ground and from space. Much of this monitoring is based on the use of remote sensing and therefore relies on the availability of reliable laboratory spectroscopic data.

Another potential use of ozone spectroscopy is provided by remote sensing of other planets, particularly exoplanets. The use of spectra of key molecules whose presence in the atmosphere of an exoplanet could point towards the possible presence of life, so-called biomarkers, is the subject of active discussion [2]. One of the most important biomarkers is the presence of methane in an oxygen-rich atmosphere [3]. As diatomic oxygen does not have a strong IR spectrum due to its symmetry, oxygen's first derivative ozone takes on the role as an important biomarker [4] alongside the O_2 A band.

Ozone can be monitored at both ultraviolet (UV) and infrared (IR) wavelengths. There are extensive compilations of spectroscopic data on ozone in general spectroscopic databases such as HITRAN [5], GEISA [6] and the UV/Vis+ spectral data base [7], as well as the specialist compilations for missions such as MIPAS [8] and the ozone-specific Spectroscopy and Molecular Properties of Ozone (SMPO) database [9]. Recommended cross sections for UV absorption by ozone are regularly reviewed [10,11] and display a reasonable measure of self-consistency [12]. The same is not true of the IR transition intensities which are neither consistent between IR or bands between the IR and UV [13].

For atmospheric retrievals and monitoring, sub-1% accuracy in intensity is highly desirable. However, the 3 to 4% inconsistency between various experimental observations of intensities of the ozone IR absorption lines represents the present state of knowledge. As described in detail by Smith et al. [13], the major inconsistency is between several measurements of the strong 10 μm

absorption IR bands, which differ by 4%. Some of these measurements give atmospheric retrievals in line with the UV observation of the Hartley band at 254 nm and some of them do not. The second important inconsistency, between retrievals based on the 10 μm bands and 5 μm bands intensities, is described by Janssen et al. [14]. Based on measurements due to Thomas et al. [15], it was shown by Janssen et al. that the concentration of ozone determined by a retrieval based on data for the 10 μm band is 2 to 3% different from that based on the 5 μm band when using spectroscopic data from HITRAN 2012 [16].

Recently Drouin et al. [17] attempted to validate the 10 μm intensities by the simultaneous measurement of IR and microwave absorption line intensities of ozone. This study confirmed the HITRAN 2012 intensities for the 10 μm band within 1.5%; however, the accuracy was limited by the signal to noise ratio of the IR data. As 10 μm band consists of two vibration bands, namely ν_1 and the much stronger ν_3 band, the signal to noise limitations should mean that for ν_3 band the discrepancy should be even less.

Finally there also appears to be a consistency problem with ozone intensities in the 3 μm region. For this band the HITRAN 2016 [5] compilation is based on measurements due to Bouazza et al [18] and the SMPO database [9]. However analysis by Toon [19] suggests that here too there are systematic differences with line intensities when compared with results for other wavelengths, in this case in the region of 9%.

The ozone molecule has been studied extensively both experimentally and theoretically, see Ref. [20] and references therein. In particular, an accurate ground state potential energy surface (PES) of ozone was determined long ago by Tyuterev and coworkers [21]. This PES was subsequently further improved [22]. More recently Tyuterev et al. [20] calculated an *ab initio* dipole moment surface (DMS) and used it to compute intensities of the 10 μm band lines belonging to the ν_1 and ν_3 band. More details of and comparisons with this work are given below.

In this paper we concentrate only on $^{16}O_3$. We present a new *ab initio* and several fitted PESs for the ground electronic state of ozone, as well as a new *ab initio* DMS constructed for the purpose of calculating the intensities of the 10 μm, 5 μm and 3 μm bands of ozone. Section 2 presents our *ab initio* PES and DMS calculations. The *ab initio* PES is constructed mainly to be the starting point for obtaining a spectroscopically-determined PES. Conversely, semi-empirical adjustment of the DMS usually leads to a deterioration in the intensity calculations [23,24]. Thus we use our *ab initio* DMS for all intensity calculations. Section 3 describes the fit of the ozone PES to spectroscopic data; we also provide a comparison of the resulting PES with the existing ones. Section 4 describes our intensity calculations which are compared to the experimental values and previous theoretical results. Section 5 gives our conclusions and plans for further work.

2. Calculation of the *ab initio* PES and DMS

A completely global, *ab initio*, ozone PES was recently constructed [25] which removed previous problems with a spurious hump in the dissociation region; this means that there is an available $^{16}O_3$ PES which is well-characterized for every geometry.

For our purposes we need both an analytical *ab initio* PES and the values of the *ab initio* energies at hundreds of geometries, as both are used in our procedure to fit the PES to experimental data; see, for example, Bubukina et al. [26]. This is because our fit procedure uses both empirical energies and *ab initio* points with a reduced weight; including these points prevents the final PES from moving too far away from the *ab initio* surface [27]. This is done in order to both avoid "holes" in the resulting PES, and to be able to fit more PES parameters than is possible when only a limited number of vibrational band origins are known.

We calculated both the PES and DMS at the same level of quantum chemical theory. Experience with calculations of the DMS for CO_2 [28] shows that, if the fundamental band origins of the molecule are predicted to better than 1 cm^{-1}, one can expect the sub-percent accuracy in the intensity calculations provided the same level of theory is used for the DMS calculation and very accurate nuclear-motion wave functions are used from a spectroscopically-determined PES.

These considerations resulted in the choice of the aug-cc-pwcVQZ basis set [29] and of the multi-reference configuration interaction (MRCI) method for both PES and DMS calculations. Specifically, we used the full-valence complete active space, in which the 12 valence electrons are free to populate all 18 valence orbitals; with this choice of active space the electronic wave function comprises 8,029 configuration state functions at the complete active space self-consistent field (CASSCF) and 109,785 ones at the MRCI level. We used the newer MRCI code implemented in the Molpro package [30] using the Celani-Werner internal contraction scheme [31,32]. Calculations at this level of theory took about 6 h per geometry running on a single modern CPU.

We performed *ab initio* calculations for 4300 geometries, 2637 of which are below 7000 cm^{-1} with respect to the bottom of the potential well. The Molpro package [30] was used for all electronic structure calculations.

We fitted the *ab initio* energies to the following functional form

$$V(S_1, S_2, S_3) = V_0 + \left[\sum_{i,j,k} K_{ijk} S_1^i S_2^j S_3^k \right] \exp[-b_1(\Delta r_1^2 + \Delta r_2^2)]$$
$$+ E_0[\exp(-2\alpha \Delta r_1) - 2\exp(-\alpha \Delta r_1)]$$
$$+ E_0[\exp(-2\alpha \Delta r_2) - 2\exp(-\alpha \Delta r_2)]$$
$$+ \exp[-b_2(\theta - \theta_e)] \qquad (1)$$

$$S_1 = (r_1 + r_2)/2 - r_e, \ S_2 = (r_1 - r_2)/2,$$
$$S_3 = \cos\theta - \cos\theta_e, \ \Delta r_i = r_i - r_e \qquad (2)$$

$E_0 = 11500$ cm^{-1}, $\alpha = 3.31$, $b_1 = 2.15$, $b_2 = 10$, $r_e = 1.282$ Å, $\theta_e = 116.88$ degrees.

Using 50 constants a root mean square (rms) for the *ab initio* energies of 1 cm^{-1} was obtained. Table 1 presents the $J = 0$ energy levels calculated using the resulting *ab initio* PES and compares them to experimental values. Details of the nuclear motion calculations for rovibrational energy levels are given in the next section.

The dipole moment points were calculated using the finite field procedure. We have demonstrated for both water [33] and carbon dioxide [28] that even though the finite field method requires more calculations, the resulting DMS is more accurate.

A polynomial functional form is used to represent the DMS:

$$\mu_x(r_1, r_2, \theta) = \sum_{i,j,k} K_{ijk}^x S_1^i S_2^j \tilde{S}_3^k \qquad (3)$$

$$\mu_y(r_1, r_2, \theta) = \sum_{i,j,k} K_{ijk}^y S_1^i S_2^j \tilde{S}_3^k \qquad (4)$$

where the angular valence coordinates differs from that used for the potential and is given by:

$$\tilde{S}_3 = \theta_e - \theta \qquad (5)$$

where the X axis bisects the valence angle, the Y axis is perpendicular to X, and the Z axis, for which $\mu_z = 0$, is perpendicular to the molecular plane. The X and Y components of the dipole were fitted separately. μ_x has the symmetry properties $\mu_x(r_1, r_2, \theta) = \mu_x(r_2, r_1, \theta)$; the indices were therefore selected by

Table 1

Observed band origins, in cm^{-1}, of $^{16}O_3$ used in the fitting procedures and differences between observed and calculated values (in cm^{-1}) for three new spectroscopically-determined potentials.

ν_1	ν_2	ν_3	E_{obs}	PES ai	PES1	PES2	PES3
0	1	0	700.9310	4.43	0.0174	0.0570	0.0627
1	0	0	1103.1370	−1.86	0.0160	0.0249	0.0291
0	2	0	1399.2730	8.70	−0.0092	−0.0120	−0.0330
1	1	0	1796.2620	2.51	0.0171	−0.0153	−0.0295
0	0	2	2057.8910	−9.38	0.0666	0.0453	0.0387
0	3	0	2094.9920	12.81	−0.0562	−0.0588	−0.1328
2	0	0	2201.1550	−3.92	−0.0103	0.0146	0.0347
1	2	0	2486.5760	6.72	−0.0499	−0.1087	−0.1443
0	1	2	2726.1070	−5.13	0.0580	0.0983	0.1096
0	4	0	2787.9000	16.66		0.5974	0.4494
2	1	0	2886.1780	0.41	−0.0228	−0.0089	−0.0205
1	0	2	3083.7030	−9.80	0.0036	0.1731	0.1679
1	3	0	3173.9290	10.77		0.4359	0.3818
3	0	0	3289.9300	−5.63	0.0073	0.0254	0.0252
0	2	2	3390.9180	−0.97	0.0346	0.0494	0.0535
0	5	0	3478.4000	20.73		0.0972	−0.0892
2	2	0	3568.0700	9.42		0.2299	0.2006
1	1	2	3739.4270	−5.63	−0.0137	0.0236	−0.0082
1	4	0	3858.6000	15.19			−1.7993
3	1	0	3966.7000	−1.43	0.0021	0.0799	0.0479
0	0	4	4001.3140	−13.92	0.0155	−0.0096	−0.0403
2	0	2	4141.4180	−0.06	0.0271	−0.0015	−0.0045
2	3	0	4246.7000	8.84		−1.0634	−1.1265
4	0	0	4370.3000	−6.76		−0.4440	−0.5366
1	2	2	4390.5000	−1.43		−0.1839	−0.2234
0	1	4	4632.8880	−2.34		−0.0333	−0.1013
3	2	0	4643.8000	−4.54		0.0761	0.0251
2	1	2	4783.4610	−9.25	−0.0460	−0.0089	−0.0272
1	0	4	4922.5720	−11.67		0.1503	0.2291
4	1	0	5038.5000	−3.08		−1.2119	−1.2083
3	0	2	5172.0000	−13.28	−0.0653	−0.4313	−0.5617
0	2	4	5266.9000	−3.06		−0.7619	−0.8423
3	3	0	5310.5000	5.94	−0.1129	0.4639	0.6248
5	0	0	5443.0000	−6.07			−3.0049
1	1	4	5540.8980	−6.23			1.6853
4	2	0	5701.6000	0.48		−0.0513	−0.1379
2	0	4	5766.3200	−9.90		0.8783	1.3582
3	1	2	5812.6000	−9.55		0.3437	0.3426
0	0	6	5997.0000	−3.61			−2.8861
5	1	0	6100.2100	−4.59		−0.4007	−0.5910
0	0	1	1042.0840	−5.10	−0.0082	−0.0696	−0.0794
0	1	1	1726.5220	−0.76	0.0054	−0.0051	0.0120
1	0	1	2110.7840	−6.45	0.0256	0.1036	0.1026
0	2	1	2407.9350	3.41	−0.0326	−0.0952	−0.0851
1	1	1	2785.2390	−2.25	0.0387	0.0256	0.0224
0	0	3	3046.0880	−12.59	0.0186	0.0639	0.0466
0	3	1	3086.2180	7.43	−0.0419	−0.1323	−0.1696
2	0	1	3186.4110	−8.92	0.0261	0.0822	0.0687
1	2	1	3455.8240	1.78	−0.0313	−0.1369	−0.1418
0	1	3	3698.2920	−8.33	−0.0006	0.0951	0.0638
2	1	1	3849.9110	−4.81	−0.0066	0.0304	0.0207
1	0	3	4021.8500	−11.70	0.0099	0.0544	0.0387
1	3	1	4122.0690	5.61		0.2899	0.2788
3	0	1	4250.2230	−10.27	−0.0069	−0.0404	−0.1484
0	2	3	4346.7270	−4.03	0.0997	0.2117	0.1666
2	2	1	4508.1320	−0.99		0.1729	0.1588
1	1	3	4658.9500	−7.15	0.0201	−0.1270	−0.1879
1	4	1	4783.2000	9.21		−0.9981	−0.9682
3	1	1	4897.2770	2.43	0.0222	−0.0288	−0.0254
0	0	5	4919.2030	−21.86		0.0359	0.0371
2	0	3	5077.0950	−4.79	−0.0087	−0.3957	−0.3887
1	2	3	5291.1710	−2.47	0.0076	0.0836	0.0483
4	0	1	5307.7900	−11.83	0.0217	−0.4022	−0.6822
0	1	5	5518.8120	−6.70		0.0990	0.2440
3	2	1	5562.0000	−1.18			−2.8649
2	1	3	5697.3230	−12.88		−0.0054	0.0216
1	0	5	5783.7850	−9.48			1.7396
4	1	1	5947.0700	−8.37		−0.7589	−0.8447
1	0	5	6063.9220	−5.57		−1.1198	−1.2258

$j = 0, 2, 4, \ldots$. For μ_y, the symmetry property is $\mu_x(r_1, r_2, \theta) = -\mu_x(r_2, r_1, \theta)$ and the indices were restricted to $j = 1, 3, 5, \ldots$.

For μ_X, 53 constants were fitted and 730 *ab initio* points were used. The root-mean-square (RMS) deviation of the fit was $\sigma = 2.64 \times 10^{-5}$ au. For μ_y, 43 constants were fitted and 2404 *ab initio* points were used. The RMS deviation of the fit was almost identical, $\sigma = 2.65 \times 10^{-5}$ au. A Fortran file containing the DMS is presented in the supplementary material.

3. Fitting the PES to experimental energy levels

In many different cases, such as for recent calculation for water [34], it has been shown that the accuracy of the predicted intensities for computed absorption lines depends on the quality of the wave functions used to represent the lower and upper states in the corresponding transitions. Our *ab initio* PES is not good enough if we want to aim for intensity predictions accurate to better than 1%. Thus fitting of the PES to empirical energy levels is necessary. The *ab initio* PES was then fitted to selected experimental energy levels using an iterative procedure based on the method developed by Yurchenko et al. [27].

Studies on the water molecule [34] have shown that a significantly more accurate PES can be obtained if we limit ourselves to a restricted set of empirical energy levels. In particular for water, the highest energy involved in the fitting procedure [34] was 15 000 cm^{-1}, whereas the levels known from conventional spectroscopy extends to 26 000 cm^{-1}; indeed multi-resonance spectra [35,36] even reach and go beyond dissociation [37]. If we do not aim at completeness or to cover all the available experimental data and concentrate on the lower energies, significantly more accurate results can be obtained. In particular, for H$_2^{16}$O when we fitted the data up to 26 000 cm^{-1} [26], the standard deviation of the fit was about 0.025 cm^{-1}. While limiting energies to below 15 000 cm^{-1}, more than a twofold improvement in accuracy was achieved with a standard deviation of 0.011 cm^{-1} [34]. Here we opted to fit data significantly higher than the energies of the bands we are interested in, but lower than the highest experimentally known energy levels.

3.1. Nuclear motion calculations

The nuclear-motion Schrödinger equation was solved using program DVR3D [38], which makes use of an exact kinetic energy operator. These calculations were performed in Radau coordinates and used Morse-like oscillators [39] with the values of parameters $r_e = 2.8$, $D_e = 0.1$ and $\omega_e = 0.0024$ in atomic units for both radial coordinates, and associated Legendre functions for the angular coordinate as basis functions. The corresponding DVR grids contained 20, 20 and 70 points for these coordinates, respectively. The final diagonalized vibrational matrices had dimension 1500. For the rotational problem, the dimensions of the final matrices were obtained using the expression $400(J + 1 - p)$, where J is the total angular momentum quantum number and p is the value of parity. Atomic masses equal to 15.994915 Da were used for oxygen; using atomic rather than nuclear masses very approximately accounts for non-adiabatic effects [40].

3.2. Optimization results

Empirical $J=0$ energy levels were taken from the table in SMPO data base [9], $J=2$ and $J=5$ levels were obtained from HITRAN frequencies. This gave a total of 371 levels with energies up to 6000 cm^{-1}. We varied the values of 36 non-zero potential parameters of the starting PES, henceforth PES ai, to obtain best agreement with three separate sets of experimental energy levels; as a result, we obtained three new potentials:
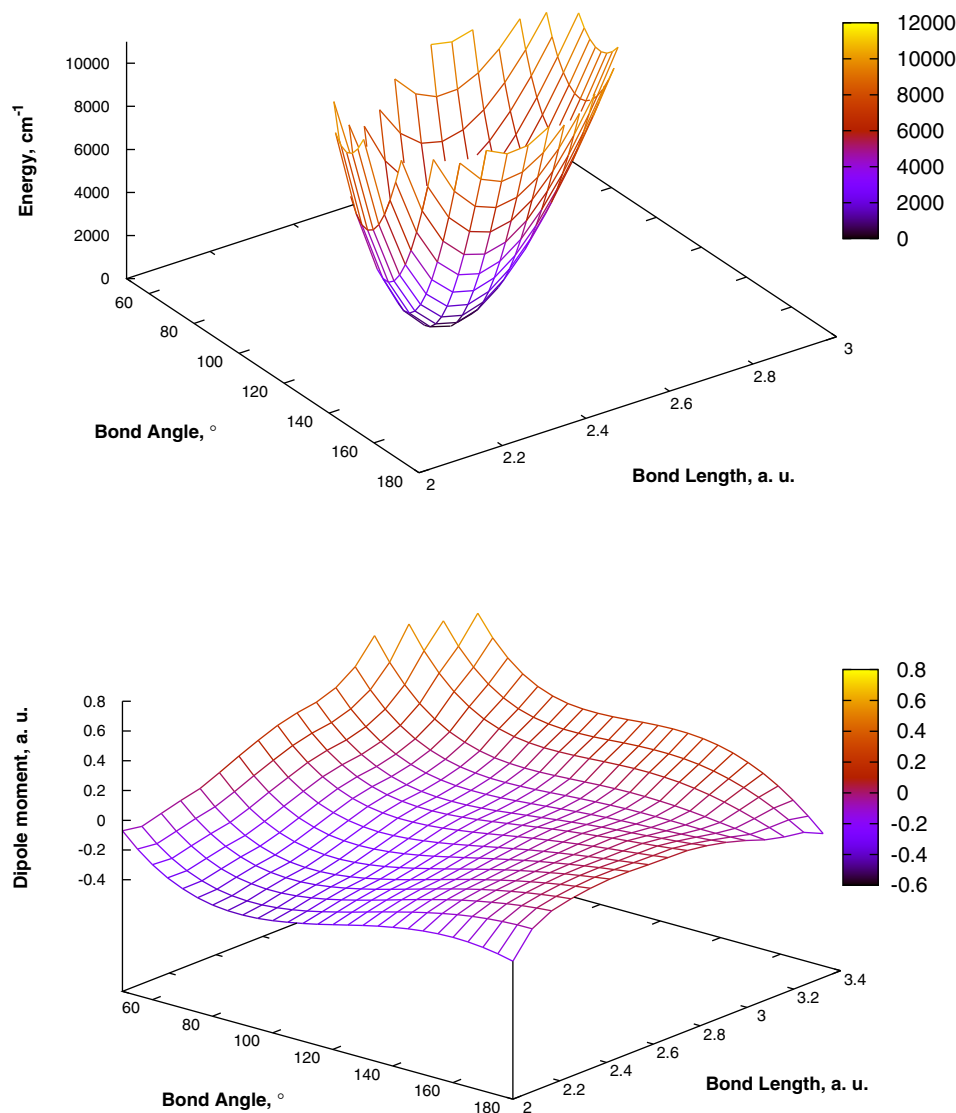
Fig. 1. Cuts through the PES1 potential (upper) and dipole moment surface (lower). Plots are for isosceles triangle geometries with both bondlengths kept the same. The DMS plot gives the "bisector" z-component of the dipole as for isosceles geometries the other components of the dipole are zero.

PES1 reproduces a set of 301 (70 were excluded from the fit) empirical energy levels with a standard deviation of 0.027 cm^{-1}.

PES2 reproduces a set of 350 (21 excluded) empirical energy levels with a standard deviation of 0.225 cm^{-1}.

PES3 reproduces the complete set of 371 empirical energy levels with a standard deviation of 0.693 cm^{-1}. This rms is dominated by the residues for so-called dark states which are only reproduced with an rms of 1.6 cm^{-1}. The other levels have an rms of 0.3 cm^{-1}.

Most of the excluded energy levels are highly excited or have high values of bending quantum number ν_2; these levels are not well-described within our method which concentrated on getting a very accurate representation of the stretching motions.

The method by Yurchenko et al. [27] allows us to optimize simultaneously with respect to both the experimental rovibrational energy levels and *ab initio* energies. This avoids creating nonphysical features in the optimized PES. For this purpose we used a set of 2637 *ab initio* electronic energies in the energy region up to 7000 cm^{-1} (about 2.4% of *ab initio* points from the original set of 2701 energies were excluded from the fit). Standard deviations of

our final PESs from this set of *ab initio* data are about 69 cm^{-1}, 87.2 cm^{-1}, and 75.1 cm^{-1}, respectively. At the final stages of our fits the weights of *ab initio* points were 3×10^{-9} for PES1 and 10^{-8} for PES2 and PES3, with the empirical data unit weighted. This was sufficient to ensure the physically correct behavior of the fitted potentials.

Table 1 presents the values of the $J = 0$ band origins calculated using the *ab initio* PES, PES1, PES2 and PES3. Fortran files representing all the PESs are provided as part of the supplementary material. Fig. 1 shows a cuts through the potential (PES1) and *ab initio* DMS.

4. Intensity of ozone absorption lines in the 10 μm, 5 μm and 3 μm bands

All absolute intensities quoted in are in "HITRAN units" of cm^2/(molecule cm) and converted to 100 % $^{16}O_3$.

In order to calculate line intensities analytical forms for both the PES and DMS must be provided to the DVR3D program suite. Comparisons were made for various PESs and DMSs: our *ab initio* DMS, PES1 and surfaces from the recent work of Tyuterev et al. [20].

Table 2

Intensities of the $^{16}O_3$ ν_3 band calculated using PESs and DMSs from Tyuterev et al. [20] and this work. HITRAN intensities are given as 100% abundance in units of cm/molecule with powers of 10 in parenthesis. Other intensities are given as a percentage difference to these values.

Assignment (001)	$\tilde{\nu}$ (cm^{-1})	HITRAN	(o-c)/c% DMS F2 [20] PES [20]	(o-c)/c% DMS F2 [20] PES1(this work)	(o-c)/c% DMS(this work) PES1(this work)
15 0 14 0	1052.848	4.09(−20)	−2.7	−3.6	0.8
17 0 16 0	1053.966	4.07(−20)	−2.7	−3.7	0.8
16 1 15 1	1053.168	4.05(−20)	−2.8	−3.7	0.8
15 1 14 1	1053.692	4.02(−20)	−2.5	−3.5	0.9
14 1 13 1	1051.985	3.99(−20)	−2.7	−3.6	0.8
17 1 16 1	1055.006	3.99(−20)	−2.6	−3.5	0.9
18 1 17 1	1054.289	3.98(−20)	−2.8	−3.7	0.8
13 0 12 0	1051.657	3.97(−20)	−2.6	−3.6	0.8
15 0 16 0	1027.456	3.97(−20)	−2.4	−3.3	1.0
14 1 15 1	1028.495	3.94(−20)	−2.4	−3.3	1.1
13 0 14 0	1029.433	3.94(−20)	−2.4	−3.3	1.0
19 0 18 0	1055.016	3.93(−20)	−2.8	−3.7	0.8
16 1 17 1	1026.476	3.92(−20)	−2.4	−3.2	1.1
13 1 12 1	1052.308	3.91(−20)	−2.5	−3.5	0.9
17 0 18 0	1025.426	3.89(−20)	−2.4	−3.3	1.1
19 1 18 1	1056.244	3.84(−20)	−2.7	−3.6	0.9
12 1 13 1	1030.463	3.83(−20)	−2.3	−3.3	1.0
16 2 15 2	1053.680	3.81(−20)	−2.7	−3.6	0.8
15 2 14 2	1053.520	3.81(−20)	−2.6	−3.5	0.9
17 2 16 2	1054.968	3.81(−20)	−2.6	−3.5	0.9
20 1 19 1	1055.350	3.80(−20)	−2.9	−3.7	0.8
15 1 16 1	1027.103	3.79(−20)	−2.6	−3.5	0.9
12 1 11 1	1050.741	3.79(−20)	−2.6	−3.6	0.8
18 1 19 1	1024.406	3.79(−20)	−2.3	−3.6	0.7
13 1 14 1	1029.095	3.78(−20)	−2.6	−3.5	0.9
11 0 12 0	1031.360	3.76(−20)	−2.4	−2.2	1.0
14 2 13 2	1052.392	3.75(−20)	−2.7	−3.6	0.8
18 2 17 2	1054.911	3.75(−20)	−2.8	−3.6	0.9
11 0 10 0	1050.385	3.71(−20)	−2.6	−3.6	0.8
19 0 20 0	1023.342	3.70(−20)	−2.4	−3.2	1.1
21 0 20 0	1056.007	3.69(−20)	−2.9	−3.7	0.8
17 1 18 1	1025.073	3.69(−20)	−2.6	−3.4	0.9
19 2 18 2	1056.376	3.69(−20)	−2.7	−3.5	0.9
13 2 12 2	1052.043	3.68(−20)	−2.5	−3.5	0.9
14 2 15 2	1028.139	3.65(−20)	−2.4	−3.4	1.0
11 1 10 1	1050.863	3.64(−20)	−2.4	−3.5	0.9
16 2 17 2	1026.120	3.62(−20)	−2.5	−3.4	1.0
11 1 12 1	1031.051	3.62(−20)	−2.5	−3.5	0.9
15 2 16 2	1026.979	3.62(−20)	−2.6	−3.4	0.9
21 1 20 1	1057.397	3.60(−20)	−2.7	−3.6	0.9
13 2 14 2	1029.002	3.59(−20)	−2.5	−3.5	0.9
20 2 19 2	1056.081	3.58(−20)	−2.9	−3.6	0.8
10 1 11 1	1032.381	3.57(−20)	−2.3	−3.3	1.0
20 1 21 1	1022.285	3.56(−20)	−2.4	−3.9	0.9
12 2 11 2	1051.047	3.55(−20)	−2.6	−3.6	0.9
12 2 13 2	1030.115	3.54(−20)	−2.4	−3.4	1.0
22 1 21 1	1056.351	3.54(−20)	−3.0	−3.7	0.7
17 2 18 2	1024.922	3.52(−20)	−2.6	−3.5	0.9
18 2 19 2	1024.056	3.49(−20)	−2.6	−3.3	1.0
19 1 20 1	1023.003	3.49(−20)	−2.7	−3.4	0.9

Tables 2 and 3 present comparisons of calculated intensities with empirical data used in HITRAN 2016 and which are taken from the SMPO [9] database. Table 2 presents a comparison of the calculated intensities using DMS F2 of Tyuterev et al. [20] and our DMS using the wave functions produced by our PES1 for the 10 μm (001) band which is ozone's strongest IR band. Comparison of the results shows that use of DMS F2 gives results that differ from those given by our DMS by almost 4% when the same PES is used. We do not have access to the PES used by Tyuterev et al. [20], hence we cannot present the results using their PES and our DMS. The results using their PES and DMS are therefore taken from the table X of their paper [20]. The difference with our results (last column) is slightly lower – only 3%. It would seem that the difference of 4% between different DMSs is compensated by about 1% due to the use of different PESs. The discrepancy with experiment given by our PES1 and DMS is significantly lower than other combinations: less than 1%.

Table 3 gives a similar comparison for the much weaker (100) band at 9 μm. The difference between calculations performed with Tyuterev et al.'s DMS F2 and our DMS is the same 4 %. However, for this band the discrepancy with HITRAN 2016 is slightly worse in our calculations.

Results for the 5 μm (101) band line intensities are presented in the Table 4. One can see that as for the strong (001) 10 μm band, that our 5 μm band predicted intensities agree with the observed intensities within the experimental uncertainties [15].

The last region of interest for the problem of retrieval inconsistencies is 2900 cm^{-1} – 3000 cm^{-1} region. As reported by Toon [19] "The 2900–3000 cm^{-1} also produce 8–9% too low $^{16}O_3$ amounts in all line lists." This means that intensities of the experi-

Table 3

Intensities of the $^{16}O_3$ ν_1 band calculated using PESs and DMSs from Tyuterev et al. [20] and this work. HITRAN intensities are given as 100% abundance in units of cm/molecule with powers of 10 in parenthesis. Other intensities are given as a percentage difference to these values.

Assignment (100)	$\tilde{\nu}$ (cm^{-1})	HITRAN	(o-c)/c% DMS F2 [20] PES [20]	(o-c)/c% DMS F2 [20] PES1(this work)	(o-c)/c% DMS(this work) PES1(this work)
25 1 24 0	1123.946	2.04(−21)	2.3	1.4	5.4
26 0 25 1	1124.295	2.03(−21)	2.1	1.3	5.3
24 0 23 1	1122.544	2.01(−21)	2.4	0.8	6.4
27 1 26 0	1125.524	2.01(−21)	2.0	1.2	5.0
23 1 22 0	1122.401	1.99(−21)	2.6	1.7	5.6
28 0 27 1	1126.022	1.98(−21)	1.9	1.1	5.1
22 0 21 1	1120.763	1.95(−21)	2.7	1.8	5.7
29 1 28 0	1127.129	1.93(−21)	1.8	1.1	5.1
21 1 20 0	1120.899	1.88(−21)	2.9	2.0	5.9
30 0 29 1	1127.731	1.87(−21)	1.6	1.1	5.0
20 0 19 1	1118.945	1.80(−21)	3.0	2.1	6.0
31 1 30 0	1128.752	1.79(−21)	1.5		4.9
32 0 31 1	1129.426	1.72(−21)	1.4		5.7
19 1 18 0	1119.446	1.70(−21)	3.2	2.3	6.2
18 0 17 1	1117.083	1.60(−21)	3.3	2.4	6.3
32 0 31 1	1129.426	1.72(−21)	1.2	1.7	5.7
34 0 33 1	1131.110	1.54(−21)	3.6		4.6
17 1 16 0	1118.049	1.48(−21)	1.1	2.7	6.5
35 1 34 0	1132.024	1.44(−21)	3.7		4.7
16 0 15 1	1115.177	1.35(−21)	1.1	2.8	6.6
36 0 35 1	1132.786	1.34(−21)	0.9		4.6
37 1 36 0	1133.671	1.24(−21)	4.0		4.6
15 1 14 0	1116.703	1.22(−21)	0.8	3.1	6.8
38 0 37 1	1134.454	1.14(−21)	1.9		4.5
28 1 27 2	1123.772	1.11(−21)	2.0	1.3	5.3
29 2 28 1	1129.009	1.10(−21)	1.8	1.3	5.3
30 1 29 2	1125.905	1.10(−21)	2.3	1.1	5.2
27 2 26 1	1127.967	1.09(−21)	2.3	1.4	5.4
26 1 25 2	1121.562	1.09(−21)	4.1	1.4	5.5
14 0 13 1	1113.231	1.08(−21)	1.8	3.3	7.0
31 2 30 1	1130.139	1.07(−21)	2.4		5.1
25 2 24 1	1127.001	1.06(−21)	1.6	2.6	6.5
32 1 31 2	1127.953	1.05(−21)	0.7	0.9	5.0
39 1 38 0	1135.318	1.05(−21)	2.4		4.5
24 1 23 2	1119.287	1.03(−21)	1.6	1.6	5.6
33 2 32 1	1131.357	1.01(−21)	2.8	1.0	5.0
23 2 22 1	1126.090	9.75(−22)	1.4	1.9	5.8
34 1 33 2	1129.918	9.65(−22)	4.5		4.9
13 1 12 0	1115.399	9.61(−22)	0.6	3.6	
40 0 39 1	1136.114	9.50(−22)	2.6		
22 1 21 2	1116.967	9.44(−22)	1.3	1.8	5.8
35 2 34 1	1132.657	9.17(−22)	3.1		4.9
21 2 20 1	1125.209	8.81(−22)	1.2	2.2	6.0
36 1 35 2	1131.808	8.65(−22)	0.5		4.9
41 1 40 0	1136.964	8.60(−22)	2.9		
20 1 19 2	1114.626	8.35(−22)	4.6	2.1	6.0
12 0 11 1	1111.255	8.19(−22)	1.1	3.8	
37 2 36 1	1134.029	8.10(−22)	3.5		4.8
19 2 18 1	1124.329	7.74(−22)	0.4	2.5	6.3
42 0 41 1	1137.768	7.74(−22)	1.0		4.4
38 1 37 2	1133.632	7.52(−22)			4.8

mental lines presented in these line lists are too large by about 9%. Table 5 presents intensities for the (003) band. It can be seen that our calculated intensities are between 7 and 11% lower than the HITRAN values. This indicates that our calculated intensities should solve the 3000 cm^{-1} region inconsistency problem as well. We note that our results show a distinct difference between P-branch transitions (difference relative to HITRAN about 7%) and R-branch ones (difference 11%). At this stage it is unclear if this issue is associated with the measurements or our calculations.

5. Conclusions

This work addresses from a theoretical perspective the long standing problem of inconsistency of the IR intensities of ozone.

For the 10 μm band, for which different laboratory measurements yield results which differ by up to 4%, our calculations coincide within 1% with the measurements selected by HITRAN and confirmed recently by simultaneous microwave and infrared measurements [17]. Furthermore, our calculations for absorption lines in the 5 μm band using the same surfaces gives results within the experimental accuracy of about 2%. Finally, our results for 3 μm suggest that a significant lowering of the intensities given by HITRAN in this region is needed; this result would appear also to be in line with recent atmospheric observations [19].

The next step in this study is to produce comprehensive line lists for $^{16}O_3$ and its isotopologues, and use them as input to atmospheric radiative transfer models to demonstrate that their use does indeed lead to consistent retrievals. This involves producing

Table 4

Calculated $^{16}O_3$ intensities (PES1 and our DMS) of the (001), (100) and (101) bands compared with the measurements of Thomas et al. [15]. Measured intensities are given as 100% abundance in units of cm/molecule with powers of 10 in parenthesis. Our intensities are given as a percentage difference to these values.

$\tilde{\nu}$ (cm^{-1})	Intensity	exp. unc.%	Assign E_{up}	Assign E_{low}	(o-c)/c %
973.0979	1.94(−22)	2.3	58 2 57 (001)	59 2 58 (000)	2.6
974.5576	2.92(−22)	2.2	57 0 57 (001)	58 0 58 (000)	1.5
974.5809	2.36(−22)	1.5	57 1 56 (001)	58 1 57 (000)	0.6
974.5987	8.80(−23)	3.9	55 9 46 (001)	56 9 47 (000)	−1.9
988.8183	1.07(−21)	0.8	47 5 42 (001)	48 5 43 (000)	0.6
994.5107	1.09(−21)	1.1	39 10 29 (001)	40 10 30 (000)	0.2
1048.6125	1.53(−21)	1.6	19 13 6 (001)	18 13 5 (000)	0.6
1051.3383	1.15(−21)	0.8	27 12 15 (001)	26 12 14 (000)	
1054.0585	1.63(−21)	1.6	23 12 11 (001)	22 12 10 (000)	1.0
1058.0241	1.27(−21)	1.5	36 11 26 (001)	35 11 25 (000)	0.0
1059.5267	1.99(−21)	1.1	36 10 27 (001)	35 10 26 (000)	0.1
1065.9838	1.63(−21)	1.4	44 7 38 (001)	43 7 37 (000)	−0.1
1066.0126	2.14(−21)	1.5	47 1 46 (001)	46 1 45 (000)	−0.8
1070.4355	1.83(−21)	1.4	47 3 44 (001)	46 3 43 (000)	0.4
1071.0834	1.71(−21)	1.0	47 4 43 (001)	46 4 42 (000)	
1071.9168	1.19(−21)	0.8	49 4 45 (001)	48 4 44 (000)	0.0
1077.9813	3.69(−22)	1.1	33 8 26 (100)	32 9 23 (000)	4.5
1078.8580	3.44(−22)	1.2	30 0 30 (100)	31 1 31 (000)	−4.9
1079.4090	4.06(−22)	0.9	20 6 14 (100)	19 7 13 (000)	4.8
1083.0592	3.39(−22)	1.3	17 5 13 (100)	16 6 10 (000)	5.2
1100.0901	5.00(−22)	0.8	22 3 19 (100)	21 4 18 (000)	4.5
1101.7616	4.93(−22)	0.7	25 3 23 (100)	24 4 20 (000)	4.5
1104.0767	4.94(−22)	0.9	26 3 23 (100)	25 4 22 (000)	4.4
1109.2699	5.71(−22)	0.7	10 0 10 (100)	9 1 9 (000)	6.7
1111.5000	3.25(−22)	1.4	7 1 7 (100)	6 0 6 (000)	8.2
1115.1773	1.32(−21)	0.7	16 0 16 (100)	15 1 15 (000)	4.2
1116.7032	1.20(−21)	1.2	15 1 15 (100)	14 0 14 (000)	5.3
1118.0486	1.45(−21)	1.1	17 1 17 (100)	16 0 16 (000)	4.6
1119.2868	1.02(−21)	0.8	24 1 23 (100)	23 2 22 (000)	4.4
1119.4463	1.67(−21)	1.0	19 1 19 (100)	18 0 18 (000)	4.3
1121.5617	1.07(−21)	0.9	26 1 25 (100)	25 2 24 (000)	3.7
1122.4009	1.95(−21)	1.3	23 1 23 (100)	22 0 22 (000)	3.6
1122.5439	1.98(−21)	1.3	24 0 24 (100)	23 1 23 (000)	3.3
1123.8503	1.51(−22)	1.0	6 3 3 (100)	5 2 4 (000)	8.2
1123.9457	2.00(−21)	1.2	25 1 25 (100)	24 0 24 (000)	3.6
1124.2947	1.99(−21)	1.3	26 0 26 (100)	25 1 25 (000)	3.2
1124.3286	7.61(−22)	1.0	19 2 18 (100)	18 1 17 (000)	4.5
1126.6751	4.60(−22)		36 2 34 (100)	35 3 33 (000)	5.5
1127.2348	2.64(−22)		10 3 7 (100)	9 2 8 (000)	8.1
1129.2358	3.53(−22)		13 3 11 (100)	12 2 10 (000)	7.0
1129.2765	1.37(−22)		5 4 2 (100)	4 3 1 (000)	8.9
1132.6569	9.07(−22)	0.5	35 2 34(100)	34 1 33 (000)	3.7
1132.7860	1.33(−21)	0.5	36 0 36 (100)	35 1 35 (000)	3.6
1132.8114	4.83(−22)	0.7	19 3 17 (100)	18 2 16 (000)	5.7
1133.4335	2.65(−22)	0.7	10 4 6 (100)	9 3 7 (000)	8.1
1133.5869	1.37(−22)	1.2	18 2 16 (100)	17 1 17 (000)	5.2
1133.6317	7.44(−22)	1.1	38 1 37 (100)	37 2 36 (000)	3.6
1133.6712	1.23(−21)	1.0	37 1 37 (100)	36 0 36 (000)	3.7
1133.7245	5.04(−22)	0.4	21 3 19 (100)	20 2 18 (000)	4.5
1133.9786	3.02(−22)	1.4	42 2 40 (100)	41 3 39 (000)	3.1
1134.0288	8.00(−22)	1.2	37 2 36 (100)	36 1 35 (000)	3.4
1134.2514	2.91(−22)	0.6	11 4 8 (100)	10 3 7 (000)	7.5
2086.1304	4.94(−22)	0.5	19 10 9 (101)	20 10 10 (000)	−1.4
2086.4723	8.82(−22)	0.5	21 8 13 (101)	22 8 14 (000)	−2.1
2086.9846	3.64(−22)	0.9	18 9 10 (101)	19 9 11 (000)	−1.0
2087.5873	9.23(−22)	0.8	20 8 13 (101)	21 8 14 (000)	−1.4
2088.2490	3.68(−22)	0.3	17 9 8 (101)	18 9 9 (000)	−0.8
2088.6874	9.44(−22)	0.5	19 8 11 (101)	20 8 12 (000)	−2.0
2089.7729	9.59(−22)	0.7	18 8 11 (101)	19 8 12 (000)	−2.4
2103.2106	7.43(−22)	0.4	12 12 1 (101)	12 12 0 (000)	−0.7
2106.5742	8.25(−22)	0.2	14 8 7 (101)	14 8 6 (000)	−2.3
2116.8712	4.77(−22)	0.7	15 10 5 (101)	14 10 4 (000)	−1.7
2116.9201	9.11(−22)	0.8	11 7 4 (101)	10 7 3 (000)	−2.8
2117.4047	5.21(−22)	0.7	16 10 7 (101)	15 10 6 (000)	−1.8
2117.9200	5.54(−22)	0.9	17 10 7 (101)	16 10 6 (000)	−1.7
2125.2044	6.59(−22)	0.7	26 8 19 (101)	25 8 18 (000)	−5.2
2125.6791	6.33(−22)	2.0	27 8 19 (101)	26 8 18 (000)	
2132.7605	1.97(−22)	0.9	44 5 40 (101)	43 5 39 (000)	−3.6
2132.8026	2.36(−22)	1.0	43 5 38 (101)	42 5 37 (000)	−1.2

Table 5

Calculated intensities (PES1 and our DMS) of the $^{16}O_3$ (003) band compared with the HITRAN 2016. HITRAN intensities are given as 100% abundance in units of cm/molecule with powers of 10 in parenthesis. Our intensities are given as a percentage difference to these values.

$\tilde{\nu}$ (cm^{-1})	intensity HITRAN	Assignment upper	Assignment lower	(o–c)/c %
3002.8414	1.39(−22)	32 2 31 (003)	33 2 32 (000)	10.1
3007.9106	1.73(−22)	29 3 26 (003)	30 3 27 (000)	10.8
3014.1642	2.41(−22)	25 3 22 (003)	26 3 23 (000)	10.7
3020.9156	3.46(−22)	21 1 20 (003)	22 1 21 (000)	11.5
3022.5631	3.78(−22)	20 1 20 (003)	21 1 21 (000)	11.3
3025.3709	4.04(−22)	18 1 18 (003)	19 1 19 (000)	11.2
3036.4846	3.73(−22)	9 0 9 (003)	10 0 10 (000)	10.2
3050.7231	2.50(−22)	7 2 5 (003)	6 2 4 (000)	8.3
3052.3788	3.14(−22)	11 3 8 (003)	10 3 7 (000)	7.8
3056.9845	3.93(−22)	19 1 18 (003)	18 1 17 (000)	7.8
3057.6913	3.27(−22)	23 1 22 (003)	22 1 21 (000)	7.2
3057.7125	2.46(−22)	27 1 26 (003)	26 1 25 (000)	6.4

multiple line lists for each isotopologue as a check on line-by-line accuracy and stability [41,42]. Work in this direction is currently in progress.

The most important absorption of solar radiation by ozone is in the UV. The consistency between IR and UV intensity measurements is a major outstanding problem of ozone spectroscopy. An important step towards resolving this consistency problem would be achieved with the accurate (within 1%) computation of both IR and UV bands absorption. For the UV intensity calculation several components are necessary. A program to compute rovibronic transition intensities for triatomic molecules has been published recently by one of us [43]. An accurate ground electronic state PES is an important part of the electronic spectra calculations; this is presented here. Accurate *ab initio* calculated transition dipole moment surfaces and electronic excited states PES are available in the literature [44]. Fitting of the excited-state PES to experimental data and further improvement of the dipole moment calculations are in progress. This should yield accurate electronic transition intensities calculations. Again, part of this procedure is the accurate ground electronic state PES, presented in this work.

We include as supplementary material the fitted ozone PES. We searched the literature carefully and failed to find any freely available ozone PES which had been accurately fitted to reproduce the known empirical energy levels of the ozone ground electronic state, though results using such PESs have been presented many times. Thus, the present PES, given in the supplementary material as a Fortran program, is the first freely-available, accurate $^{16}O_3$ PES for ozone.

Acknowledgment

Supplementary material

Supplementary material associated with this article can be found, in the online version, at 10.1016/j.jqsrt.2018.02.018.

References

[1] Solomon S. Stratospheric ozone depletion: a review of concepts and history. Rev Geophys 1999(37):275–316. doi:10.1029/1999RG900008.

[2] France K, Linsky JL, Loyd ROP. The ultraviolet radiation environment in the habitable zones around low-mass exoplanet host stars. Astron Astrophys Suppl 2014;354:3–7. doi:10.1007/s10509-014-1947-2.

[3] Sagan C, Thompson WR, Carlson R, Gurnett D, Hord C. A search for life on earth from the Galileo spacecraft. Nature 1993;365:715–21. doi:10.1038/365715a0.

[4] Grenfell JL, Gebauer S, Godolt M, Palczynski K, Rauer H, Stock J, von Paris P, Lehmann R, Selsis F. Potential biosignatures in super-earth atmospheres II. photochemical responses. Astrobiology 2013;13:415–38. doi:10.1089/ast.2012.0926.

[5] Gordon IE, Rothman LS, Hill C, Kochanov RV, Tan Y, Bernath PF, Birk M, Boudon V, Campargue A, Chance KV, Drouin BJ, Flaud JM, Gamache RR, Hodges JT, Jacquemart D, Perevalov VI, Perrin A, Shine KP, Smith MAH, Tennyson J, Toon GC, Tran H, Tyuterev VG, Barbe A, Császár AG, Devi VM, Furtenbacher T, Harrison JJ, Hartmann JM, Jolly A, Johnson TJ, Karman T, Kleiner I, Kyuberis AA, Loos J, Lyulin OM, Massie ST, Mikhailenko SN, Moazzen-Ahmadi N, Müller HSP, Naumenko OV, Nikitin AV, Polyansky OL, Rey M, Rotger M, Sharpe SW, Sung K, Starikova E, Tashkun SA, Auwera JV, Wagner G, Wilzewski J, Wcisło P, Yu S, Zak EJ. The *hitran* 2016 molecular spectroscopic database. J Quant Spectrosc Radiat Transf 2017;203:3–69. doi:10.1016/j.jqsrt.2017.06.038.

[6] Jacquinet-Husson N, Armante R, Scott NA, Chédin A, Crépeau L, Boutammine C, Bouhdaoui A, Crevoisier C, Capelle V, Boonne C, Poulet-Crovisier N, Barbe A, Benner DC, Boudon V, Brown LR, Buldyreva J, Campargue A, Coudert LH, Devi VM, Down MJ, Drouin BJ, Fayt A, Fittschen C, Flaud J-M, Gamache RR, Harrison JJ, Hill C, Hu SM, Hodnebrog Ø, Jacquemart D, Jolly A, Jiménez E, Lavrentieva NN, Liu AW, Lodi L, Lyulin OM, Massie ST, Mikhailenko S, Müller HSP, Naumenko OV, Nikitin A, Nielsen CJ, Orphal J, Perevalov VI, Perrin A, Polovtseva E, Predoi-Cross A, Rotger M, Ruth AA, Yu SS, Sung K, Tashkun SA, Tennyson J, Tyuterev VG, Vander Auwera J, Voronin BA, Makie A, Mol J. The 2015 edition of the GEISA spectroscopic database. J Mol Spectrosc 2016;327:31–72. doi:10.1016/j.jms.2016.06.007.

[7] Noelle A, Hartmann GK, Fahr A, Lary D, Lee YP, Limao-Vieira P, Locht R, Martin-Torres FJ, McNeill K, Orlando JJ, Salama F, Vandaele AC, Wayne RP, Brunger M. UV/vis+ spectra data base. 2017. 11th Edition.

[8] Flaud JM, Piccolo C, Carli B, Perrin A, Coudert LH, Teffo JL, Brown LR. Molecular line parameters for the MIPAS (michelson interferometer for passive atmospheric sounding) experiment. Atmos Oceanic Opt 2003;16:172–82.

[9] Babikov Y, Mikhailenko SN, Barbe A, Tyuterev VG. S&MPO - an information system for ozone spectroscopy on the WEB. J Quant Spectrosc Radiat Transf 2014;145:169–80.

[10] Orphal J, Chance K. Ultraviolet and visible absorption cross-sections for HITRAN. J Quant Spectrosc Radiat Transf 2003;82:491–504. doi:10.1016/S0022-4073(03)00173-0.

[11] Orphal J, Staehelin J, Tamminen J, Braathen G, De Backer MR, Bais A, Balis D, Barbe A, Bhartia PK, Birk M, Burkholder JB, Chance K, von Clarmann T, Cox A, Degenstein D, Evans R, Flaud J-M, Flittner D, Godin-Beekmann S, Gorshelev V, Gratien A, Hare E, Janssen C, Kyrola E, McElroy T, McPeters R, Pastel M, Petersen M, Petropavlovskikh I, Picquet-Varrault B, Pitts M, Labow G, Rotger-Languereau M, Leblanc T, Lerot C, Liu X, Moussay P, Redondas A, Van Roozendael M, Sander SP, Schneider M, Serdyuchenko A, Veefkind P, Viallon J, Viatte C, Wagner G, Weber M, Wielgosz RI, Zehner C. Absorption cross-sections of ozone in the ultraviolet and visible spectral regions: Status report 2015. J Mol Spectrosc 2016;327:105–21. doi:10.1016/j.jms.2016.07.007.

[12] Orphal J. A critical review of the absorption cross-sections of O_3 and NO_2 in the ultraviolet and visible. J Quant Spectrosc Radiat Transf 2003;157:185–209. doi:10.1016/S1010-6030(03)00061-3.

[13] Smith MAH, Devi AM, Benner DC. The quest for ozone intensities in the 9–11 µm region: a retrospective. J Quant Spectrosc Radiat Transf 2012;113:825–8.

[14] Janssen C, Boursier C, Jeseck P, Te Y. Line parameter study of ozone at 5 and 10 µm using atmospheric FTIR spectra from the ground: a spectroscopic database and wavelength region comparison. J Mol Spectrosc 2016;326:48–59.

[15] Thomas X, Heyden PVD, De Backer-Barilly MR, Bourgeois MT, Barbe A. Infrared absolute intensities of ozone in the 10 and 5 µm spectral range: new investigations. J Quant Spectrosc Radiat Transf 2010;111:1080–8.

[16] Rothman LS, Gordon IE, Babikov Y, Barbe A, Benner DC, Bernath PF, Birk M, Bizzocchi L, Boudon V, Brown LR, Campargue A, Chance K, Cohen EA, Coudert LH, Devi VM, Drouin BJ, Fayt A, Flaud JM, Gamache RR, Harrison JJ, Hartmann JM, Hill C, Hodges JT, Jacquemart D, Jolly A, Lamouroux J, Le Roy RJ, Long DA, Lyulin OM, Mackie CJ, Massie ST, Mikhailenko S, Müller HSP, Naumenko OV, Nikitin AV, Orphal J, Perevalov V, Perrin A, Polovtseva ER, Richard C, Smith MAH, Starikova E, Sung K, Tashkun S, Tennyson J, Toon GC, Tyuterev VG, Wagner G. The *hitran* 2012 molecular spectroscopic database. J Quant Spectrosc Radiat Transf 2013;130:4–50. doi:10.1016/j.jqsrt.2013.07.002.

[17] Drouin BJ, Crowford TJ, Yu S. Validation of ozone intensities at 10 µm with THz spectrometry. J Quant Spectrosc Radiat Transf 2017;203:282–92.

[18] Bouazza S, Mikhailenko S, Barbe A, Regalia L, Tyuterev VG, Plateaux JJ. The $\nu_1 + \nu_2 + 2\nu_3$ and $_2 + 3\nu + 3$ bands of $^{16}O_3$. J Mol Spectrosc 1995;174:510–19. doi:10.1006/jmsp.1995.0019.

[19] Toon G. Evaluation of HITRAN 2016 o$_3$ linelist, (private communication). 2017. https://mark4sun.jpl.nasa.gov/report/o3_spectroscopy_evaluation_20170930.compressed.pdf.

[20] Tyuterev VG, Kochanov RV, Tashkun SA. Accurate ab initio dipole moment surfaces of ozone: first principle intensity predictions for rotationally resolved spectra in a large range of overtone and combination bands. J Chem Phys 2017;146. 064304.

[21] Tyuterev VG, Tashkun S, Jensen P, Barbe A. Determination of the effective ground state potential energy function of ozone from high-resolution infrared spectra. J Mol Spectrosc 1999;198:57–67.

[22] Tyuterev VG, Kochanov RV, Tashkun SA. Analytical representation for the ozone electronic ground state potential function in the spectroscopically accessible range and extended vibration predictions. In: Proceedings of XVII International Symposium HighRus-2012; 2012. p. 29–50.

[23] Lynas-Gray AE, Miller S, Tennyson J. Infra red transition intensities for water: a comparison of *ab initio* and fitted dipole moment surfaces. J Mol Spectrosc 1995;169:458–67.

[24] Tennyson J. Vibration-rotation transition intensities from first principles. J Mol Spectrosc 2014;298:1–6. https://doi.org/10.1016/j.jms.2014.01.012.

[25] Tyuterev VG, Kochanov R, Campargue A, Kassi S, Mondelain N, Barbe A, Starikova E, DeBacker MR, Szalay PG, Tashkun S. Does the "reef structure" at the ozone transition state towards the dissociation exist? new insight from calculations and ultrasensitive spectroscopy experiments. Phys Rev Lett 2014;113:143002–3.

[26] Bubukina II, Polyansky OL, Zobov NF, Yurchenko S. Accurate water potential energy surface. Opt Spectrosc 2011;277:346–9.

[27] Yurchenko SN, Carvajal M, Jensen P, Herregodts F, Huet TR. Potential parameters of PH_3 obtained by simultaneous fitting of ab initio data and experimental vibrational band origins. Chem Phys 2003;290:59–67.

[28] Polyansky OL, Bielska K, Ghysels M, Lodi L, Zobov NF, Hodges JT, Tennyson J. High accuracy CO_2 line intensities determined from theory and experiment. Phys Rev Lett 2015;114. 243001 https://doi.org/10.1103/PhysRevLett.114.243001.

[29] Hattig C. Optimization of auxiliary basis sets for RI-MP2 and RI-CC2 calculations: core-valence and quintuple-zeta basis sets for h to ar and QZVPP basis sets for Li to Kr. Phys Chem Chem Phys 2005;7:59–66. https://doi.org/10.1039/b415208e.

[30] MOLPRO. Werner H.-J, Knowles PJ. (version 2002.1) is a package of *ab initio* electronic structure programs designed.

[31] Celani P, Werner HJ. Multireference perturbation theory for large restricted and selected active space reference wave functions. J Chem Phys 2000;112. 5546.

[32] Shamasundar KR, Knizia G, Werner HJ. A new internally contracted multi-reference configuration interaction method. J Chem Phys 2011;135. 054101.

[33] Lodi L, Tennyson J, Polyansky OL. A global, high accuracy ab initio dipole moment surface for the electronic ground state of the water molecule. J Chem Phys 2011;135. 034113. doi: 10.1063/1.3604934.

[34] Mizus II, Kyuberis AA, Zobov NF, Makhnev VY, Polyansky OL, Tennyson J. High accuracy water potential energy surface for the calculation of infrared spectra. Phil Trans R Soc London A 2018;376. 20170149. doi: 10.1098/rsta.2017.0149.

[35] Grechko M, Maksytenko P, Zobov NF, Shirin SV, Polyansky OL, Rizzo TR, Boyarkin OV. Collisionally assisted spectroscopy of water from 27 000 to 34 000 cm^{-1}. J Phys Chem A 2008;112. 10539.

[36] Maksytenko P, Zobov N, Shirin SV, Polyansky OL, Muenter JS, Rizzo TR, Boyarkin OV. Approaching the full set of energy levels of water. J Chem Phys 2007;126. 241101.

[37] Zobov NF, Shirin SV, Lodi L, Silva BC, Tennyson J, Császár AG, Polyansky OL. First-principles rotation-vibration spectrum of water above dissociation. Chem Phys Lett 2011;507:48–51.

[38] Tennyson J, Kostin MA, Barletta P, Harris GJ, Polyansky OL, Ramanlal J, Zobov NF. DVR3d: a program suite for the calculation of rotation-vibration spectra of triatomic molecules. Comput Phys Commun 2004;163:85–116.

[39] Tennyson J, Sutcliffe BT. The ab initio calculation of the vibrational-rotational spectrum of triatomic systems in the close-coupling approach, with KCN and H_2Ne as examples. J Chem Phys 1982;77:4061–72. doi:10.1063/1.444316.

[40] Watson JKG. The inversion of diatomic born-oppenheimer-breakdown corrections. J Mol Spectrosc 2004;223:39–50. doi:10.1016/j.jms.2003.09.007.

[41] Lodi L, Tennyson J. Line lists for $H_2^{18}O$ and $H_2^{17}O$ based on empirically-adjusted line positions and ab initio intensities. J Quant Spectrosc Radiat Transf 2012;113:850–8. doi:10.1016/j.jqsrt.2012.02.023.

[42] Zak E, Tennyson J, Polyansky OL, Lodi L, Tashkun SA, Perevalov VI. A room temperature CO_2 line list with *ab initio* computed intensities. J Quant Spectrosc Radiat Transf 2016;177:31–42. doi:10.1016/j.jqsrt.2015.12.022.

[43] Zak EJ, Tennyson J. Ro-vibronic transition intensities for triatomic molecules from the exact kinetic energy operator; electronic spectrum for the $\tilde{C}^1B_2 \leftarrow \tilde{X}^1A_1$ transition in SO_2. J Chem Phys 2017;147. 094305. doi: 10.1063/1.4986943.

[44] Schinke R, McBane G. Photodissociation of ozone in the hartley band: potential energy surfaces, nonadiabatic couplings, and singlet/triplet branching ratio. J Chem Phys 2010;132. 044305.